Engineered Science
DOI: https://dx.doi.org/10.30919/es1890

Effect of Silver Concentration on the Photocatalytic Activity of a Nanocomposite Based on Titanium Dioxide Nanorods and Reduced Graphene Oxide

A. Kayumova,[1] P. Zhanbirbayeva,[1] A. Kuanyshbekova,[1] A. Baltabekov,[1] N. Ibrayev,[1] Zh. Idrisheva[2] and T. Serikov[1,*]

Abstract

This study investigates the influence of Ag nanoparticle concentration on the photocatalytic activity of films made of titanium dioxide nanorods (TNR) and reduced graphene oxide (rGO) sheets. TNRs were synthesised using a hydrothermal method. Using chemical reduction, Ag nanoparticles with varying concentrations and diameters of 5–12 nm were obtained on the surface of TNR. The rGO sheets were deposited onto the surface of TNR and Ag nanoparticles from a phosphate solution using an electrochemical method. From SEM images, it was established that as a result of hydrothermal synthesis, TNRs with a length of ~3.2 μm and an average diameter of 50-70 nm are formed on the surface of the substrate, and Ag nanoparticles and rGO sheets are evenly distributed over their surface. XRD and Raman spectroscopy methods confirmed the preservation of the rutile phase of TNR and the successful incorporation of Ag and rGO into the nanocomposite structure. The increase in the concentration of Ag nanoparticles on the surface of TNR and rGO leads to an expansion of spectral sensitivity in the visible range from 300 to 480 nm due to intrinsic absorption and the surface plasmon resonance (SPR) effect, which results in a decrease in the bandgap width from 3.3 eV to 2.9 eV. In addition, by adding Ag nanoparticles and rGO sheets to the TNR structure, it was possible to reduce the resistance to transfer of charge carriers by 20 times and the effective electron lifetime by 2.7 times. The photocatalytic activity of the nanocomposites was evaluated based on the degradation of methylene blue (MB), Congo red (CR) and rhodamine B (RhB) dyes. The rate of dye degradation increased with increasing concentrations of Ag nanoparticles and rGO incorporation, and was 3.2, 3.1 and 1.4 times higher for MB, CR, and RhB, respectively, compared to pure TNR. Based on the results obtained, it can be assumed that the introduction of Ag plasmonic nanoparticles increases the absorptive capacity of the material, reduces its resistance, and promotes the effective separation and transport of charge carriers, which leads to an increase in their photocatalytic activity.

Keywords: Nanorods TiO_2; Reduced graphene oxide; Silver nanoparticles; Photocatalysis; Degradation of dye.
Received: 17 September 2025; Revised: 30 October 2025; Accepted: 10 November 2025
Article Type: Research article.

1. Introduction

In recent decades, with the globalisation of industrial growth and urbanisation, the problem of environmental pollution, especially of water resources, has become increasingly pressing.[1] Among various pollutants, organic compounds such as dyes, phenols, pesticides and pharmaceuticals pose a particular danger. They are highly resistant to biodegradation.[2-4] This requires the development of effective, affordable and environmentally safe methods for their removal. One of the promising directions in the field of water purification is heterogeneous photocatalysis.[5] This process allows to decompose organic molecules down to carbon dioxide and water without requiring the addition of reagents and without generating secondary waste, which makes it attractive from both scientific and practical points of view. As is known, photocatalysis is realised when a semiconductor material is excited by light quanta whose energy exceeds the width of the band gap (Eg). This leads to the transition of an electron from the valence band to the conduction band with the formation of an electron- hole. These charge carriers can participate in oxidation-reduction reactions with oxygen and water, forming active radicals ($\cdot OH, \cdot O_2^-$) capable of destroying organic pollutants. However, the efficiency of the process is largely determined by the characteristics of the photocatalyst: its spectral response, electron-hole recombination rate, surface morphology, and stability in the

---

[1] *Karaganda National Research University named after academician Ye.A. Buketov, Karaganda, 100024, Kazakhstan*
[2] *School of Geosciences, D. Serikbayev East Kazakhstan Technical University, Ust-Kamenogorsk, 070004, Kazakhstan*
[*] *Email:* *serikov-timur@mail.ru* (T. Serikov)

reaction medium.[6]

Among various photocatalysts, such as ZnO, WO_3, CdS, and Fe_2O_3, titanium dioxide (TiO_2) attracts the most attention from researchers because it is non-toxic, thermally stable, and a photochemically inert semiconductor.[7-9] Due to its high activity under the influence of ultraviolet radiation, TiO_2 is widely used to purify water and air from organic pollutants.[10,11] However, its wide forbidden zone (~3.2 eV for the anatase phase) limits absorption to only the ultraviolet region of the solar spectrum (less than 5% of total radiation). In addition, pure TiO_2 is characterised by rapid recombination of photogenerated charge carriers, which reduces the quantum yield of photochemical reactions.[12,13]

To overcome these limitations, nanostructured forms of TiO_2, in particular TNR, are being actively developed, which have a high degree of crystallinity, directed transport of charge carriers and a high specific surface area.[14] This morphology ensures effective separation of electrons and holes, improving photocatalytic activity and making TNR a perspective material for creating advanced composite photocatalysts.

One of the effective approaches is the modification of TiO_2 with nanoparticles (NPs) of precious metals, in particular silver (Ag) and carbon nanomaterials, such as rGO. Silver has the role of an electronic ‘trap’ and a plasmonic centre, which boosts the local electromagnetic field when illuminated and expands the absorption spectrum in the visible light range due to the SPR effect.[15-17] In addition, Ag NPs form ohmic contacts with TiO_2, facilitating interfacial electron transfer and reducing the probability of their recombination with holes in the valence band. At the same time, the optimal silver content is a critical parameter: at low concentrations, the plasmonic enhancement effect is poorly expressed, while an excess of Ag can lead to light shielding and blocking of active centres, reducing the overall photocatalytic activity.[18,19]

Additional improvement of TiO_2/Ag characteristics can be achieved by introducing conductive carbon materials, in particular rGO, which has high electron mobility, a large specific surface area and the ability to interact with organic molecules via π-π interactions.[20-24] The formation of the TiO_2/Ag/rGO (TAG) heterostructure contributes to more efficient separation and transfer of charge carriers: photoinduced electrons from TiO_2 migrate to rGO and then to Ag NPs, which reduces the probability of recombination processes.[25-29] This three-component structure combines the advantages of each component: TiO_2 provides photogeneration of carriers, Ag enhances visible light absorption and serves as an electron collector, and rGO promotes rapid electron transfer and increases the active surface area.[30-35]

However, excessive silver content can lead to aggregation of low-frequency components, shielding of photosensitive areas, and even an increase in recombination rate.[36,37] This highlights the importance of precisely optimising the Ag concentration to achieve maximum photocatalytic effect. In view of the above, the creation of three-component TAG nanocomposites is of particular interest, in which a synergistic effect is achieved through the combination of the photochemical, conductive and plasmonic properties of each of the components. Such composites would not only allow for the effective use of solar radiation, but also ensure stable photocatalytic activity in an aqueous environment. However, the optimal conditions for synthesis, morphological configuration, and the influence of silver and rGO concentrations on photocatalytic activity remain the subject of active research, which is the main objective of this work.

2. Experimental section

2.1 Materials

Major part of chemical reagents and materials used in this work were purchased from Sigma–Aldrich, including: titanium butylate $C_{16}H_{36}O_4Ti$ (97%), silver nitrate ($AgNO_3$, 99.998%), sodium borohydride ($NaBH_4$, 98%), FTO glass substrates (fluorine tin oxide, 7 Ω/cm^2), polyvinylpyrrolidone (PVP, M_w=40 000, 99%), hydrochloric acid (HCl, 36.5%), H_2PtCl_6 (99.9%) RhB (≥95% purity (HPLC), powder), MB (≥82%purity, powder) and CR (≥85%purity, powder). Iodolyte H30 and Meltonix film were purchased from Solaronix, rGO (99%) were purchased at Cheaptubes company.

2.2 Material preparation

2.2.1 Synthesis of TNR

TNR were synthesised using a hydrothermal method. For this purpose, 15 ml of deionised water, 15 ml of hydrochloric acid, and 0.270 ml of $C_{16}H_{36}O_4Ti$ were poured into a 50 ml vessel and mixed in an ultrasonic bath for 3 minutes. Next, pre-cleaned FTO glass substrates with conductive side facing upwards were placed in the vessel. Then, the stainless steel autoclave was hermetically sealed and placed in an oven (SNOL, Lithuania) and kept at a temperature of 180^0C for 6 hours. After cooling to room temperature, the samples were removed, thoroughly washed with deionised water and subjected to heat treatment in an oven at 500^0C for 2 hours.

2.2.2 Synthesis of TNR/Ag

Chemical reduction was used to deposit Ag NPs onto the surface of TNR films. Ag NPs were formed by recovery of silver nitrate. 0.2 g of polyvinylpyrrolidone (PVP, molecular weight 40,000) was added to 40 ml of H_2O and ethylene glycol ($C_2H_6O_2$) (1:1), then 2 mmol of $NaBH_4$ was added to the solution mixture with vigorous stirring. The TNR substrates were immersed in the vessel with the rods facing upwards and kept in an oven at a temperature of 70°C for 5 minutes. Before heating, to deposit Ag with different concentrations on the TNR surface, $AgNO_3$ with different molar masses was added to the solution: 0.5, 1.0, 1.5, 2.0 and 2.5 mmol. As a result, TNRs with different Ag NPs contents were obtained, which were thoroughly washed with deionised water and dried at room temperature.

2.2.3 Electrochemical deposition of rGO

rGO nanostructures were deposited onto the TNR/Ag surface by electrochemical deposition.[38] For this purpose, rGO (0.5 g/l) was added to a phosphate buffer solution (PBS, NaH_2PO_4 + Na_2HPO_4). To disrupt agglomerates and ensure uniform distribution of rGO in the solution, the suspension was dispersed in an ultrasonic bath for 2 hours. The process of electrochemical deposition of rGO onto the surface of TNR/Ag was carried out using a CS350 potentiostat-galvanostat (CorrTest, China) in cyclic voltammetry mode. This approach allows precise control over the formation of rGO layers on the substrate by varying the number of cycles. The voltage varied between 0 and -1.5 V at a sweep rate of 50 mV/s. The duration of one cycle is 820 seconds. Preliminary studies have shown that in one cycle with the above duration, an optimal thickness of the rGO layer is formed on the surface, at which the best photocatalytic activity of TNR is observed. The samples were labelled TAG_0.5, TAG_1.0, TAG_1.5, TAG_2.0 and TAG_2.5.

2.3 Materials characterization

The phase composition of the materials was determined using X-ray diffractograms obtained with a STOE STADI–P powder diffractometer (Germany), CuKα radiation, $\lambda = 1.54056$ Å and a range of scanning angles 2θ was 5°–80°. X-ray diffraction patterns were analysed using the PDF powder database in the WinXPow software package. Surface morphology and EDA were performed using a Mira 3MLU Tescan scanning electron microscope (Tescan, Czech Republic). The absorption spectra of all samples were measured using a SM 2203 spectrofluorometer (Solar, Belarus). The dimensions of Ag NPs were determined by dynamic light scattering using a Zetasizer particle analyser (Malvern Panalytical, United Kingdom). Impedance spectra were obtained on a potentiostat with an EIS attachment (CS350, Corrtest Instruments). The scanning range was from 100 kHz to 100 mHz, with an applied voltage amplitude of 20 mV. The substrate with the test sample and the substrate with the platinum electrode (PlatisolT/SP, Solaronix) were bonded together with a 25 µm thick polymer film (Melotonix, Solaronix). Iodide/triiodide electrolyte (Iodolyte Z-150, Solaronix) was used as a reducing agent between the substrates. The photocatalytic activity of the samples was evaluated by measuring the photoinduced current and photodegradation of MB, CR and RhB dyes. The photoconductivity was measured at an illuminated surface area of 1 cm^2 in a standard three-electrode cell using a potentiostat. Platinum film served as the counter electrode, and AgCl served as the reference electrode. The measurements were conducted in a 0.1 M NaOH electrolyte in a specially manufactured photoelectrochemical cell with a quartz window. In all experiments, an Ossila LED solar simulator (class AAA, AM 1.5 standard) was used as the source of solar radiation. Radiation intensity is 1000 W/m^2, wavelength range is 350 nm – 1000 nm.

3. Results and discussion

Fig. 1 shows SEM images of the surface morphology of nanostructured TNR film and TNR/rGO films with different concentrations of Ag NPs (b–f). Fig. 1a shows that hydrothermal synthesis results in the formation of TNRs on the substrate surface, oriented predominantly perpendicular to the substrate surface. The film thickness is ~3.0 µm. The average length of the nanorods is ~3.2 µm, and the average diameter is 50-70 nm. The surface of nanorods is smooth, homogeneous, and geometrically anisotropic. As a result of chemical reduction of silver nitrate with different molar masses (Fig. 1 b–f), spherical Ag NPs are formed on the surface of TNR. The figure illustrates that the NPs are attached to the outside surface of the nanorods and evenly spread across their entire surface. Moreover, with an increase of the molar mass of $AgNO_3$ used in the synthesis, the amount of reconstituted Ag NPs on the surface of TNR increases. When using 0.5 mmol $AgNO_3$, the amount of reconstituted Ag NPs is smaller and not covering the entire surface of the TNR. Increasing the amount of substance of $AgNO_3$ to 2.5 mmol leads to an increase in reconstituted Ag NPs and to complete coverage of the TNR surface. In addition, the figures clearly demonstrate the precipitated rGO structures. The rGO sheets cover the surface of the TNR and Ag NPs, forming a conductive network that can facilitate electron transfer and suppress electron recombination. Fig. 1g demonstrates a histogram of the size distribution of Ag NPs obtained by dynamic light scattering. The analysis was conducted on a solution in which chemical reduction of NPs occurred. The diagram shows that the solution contains NPs ranging from 5 to 12 nm. At the same time, more than 50% of Ag NPs belong to particles with a diameter of 6-8 nm. Analysis of SEM images also confirms that particles of the above sizes are present on the surface of the TNR.

Fig. 2 represents the results of the study of samples using energy-dispersive X-ray spectroscopy. The electron beam of electron gun was accelerated by high voltage and focused on the surface of the samples, the area of which is illustrated in Fig. 2g. An analysis was performed of the energy spectra of the emitted X-ray radiation arising from the interaction of the electron beam and the atoms of the samples under investigation, which are shown in Fig. 2 a–f. To obtain quantitative data, preliminary calibration of the system was performed using a reference sample.

The data presented demonstrates that the TNR sample contains O, Ti, Si, Sn, and Na atoms. The O and Ti atoms belong to titanium dioxide nanorods. The presence of Si, Sn, and Na in the sample is associated with the use of glass substrates with a conductive layer of tin oxide. The absence of other chemical elements indicates the purity of the samples obtained without impurities. When spherical Ag NPs are

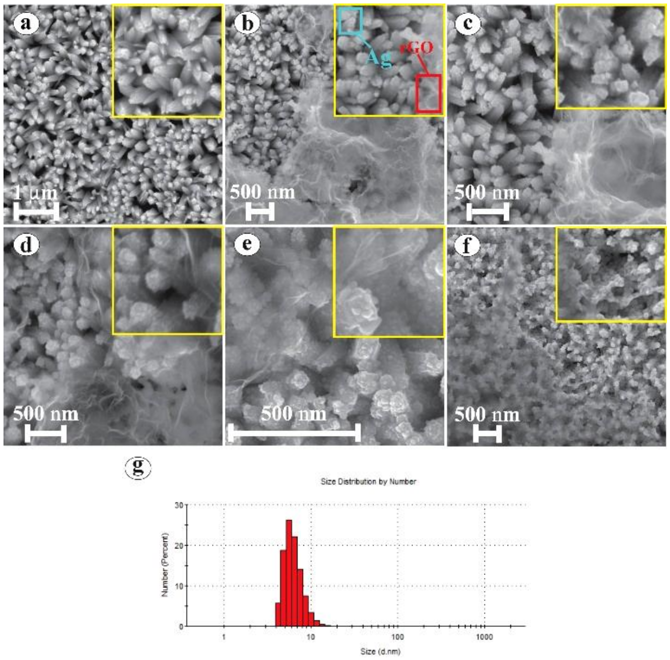

Fig. 1: SEM images of the TNR surface before and after Ag deposition: a) TNR; b) TAG_0.5; c) TAG_1.0; d) TAG_1.5; e) TAG_2.0; f) TAG_2.5; g) Histogram of Ag NPs distribution.

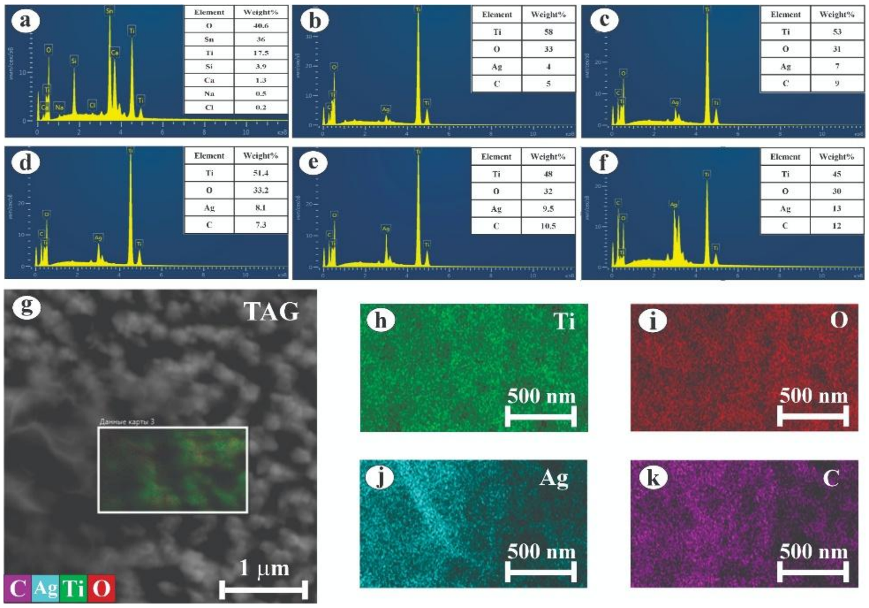

Fig. 2: EDA of TNR with deposited Ag NPs and rGO: (a) TNR; (b) TAG_0.5; (c) TAG_1.0; (d) TAG_1.5;(e) TAG_2.0; (f) TAG_2.5 and chemical element distribution map on the surface (g–k).

deposited on the TNR surface, characteristic silver peaks appear in the 3 keV region on the EDA. Quantitative analysis showed that as the molar mass of $AgNO_3$ increases, so the concentration of Ag NPs on the surface of TNR also increases. If at 0.5 mmol the proportion of Ag atoms was 4%, then at 2.5 mmol their proportion was 13% relative to all elements. All samples also contain C peaks, which are apparently associated with precipitated rGO nanostructures. Their concentration on the surface also changes. However, EDA analysis has low detection efficiency at low energies, mainly due to radiation absorption. As a rule, this leads to a strong dependence of efficiency on energy, difficulties in identifying peaks, especially low-energy ones, such as carbon.

Fig. 2g-k provides an example of a multilayer EDA map. The TAG_1.5 sample map is shown as an example. The presented map shows that Ag NPs, O, and Ti are evenly distributed across the entire surface, indicating the homogeneity of the obtained structures. C atoms are mainly concentrated in the rGO area, which also contains residual amounts of oxygen.

Fig. 3a presents X-ray diffraction patterns showing diffraction peaks for three samples: FTO substrate, TNR, and TAG. The reflections of the FTO substrates correspond to the 2θ angle positions and have the following values: 26.1°, 33.96°, 37.96°, 51.76°, 61.76° and 65.76°, which correspond to the powder diffraction standards of JCPDS No. 18–1387. In the TNR sample, the main reflections identified by the planes R(110), R(101), R(111), R(211), R(002), R(220), R(301) correspond to the rutile phase of TiO_2 (JCPDS No. 21–1276).[39] The TAG sample additionally registers peaks characteristic of Ag, corresponding to the Ag (111), Ag (200), Ag (220), and Ag (311) planes, confirming the successful incorporation of silver into the composite material. As is known, the diffraction peak of rGO is observed at 26.6°, corresponding to reflections (002), and a d-spacing value of 0.336 nm. However, the presence of broad and less intense peaks associated with rGO is difficult to distinguish due to their low intensity and overlap with the TiO_2 and Ag peaks.[40,41]

The study was conducted for all samples, however, an increase in the concentration of Ag NPs does not lead to change in diffraction peaks.

Fig. 3b presents the Raman spectra of TNR samples, TNR with deposited Ag NPs (TA) and rGO (TAG). For the initial TNR sample, intense peaks are observed at 235, 445, and 610 cm^{-1}, which correspond to the B_{1g}, E_g, and A_{1g} vibrational modes of the rutile phase of TiO_2. This confirms that the obtained TNRs are predominantly crystallised in the rutile modification with a high degree of orderliness. In the TNR spectrum with precipitated Ag NPs, the same characteristic bands of rutile-modified TiO_2 are preserved, but their intensity decreases and the peaks widen slightly, indicating the interaction of Ag NPs with the TiO_2 surface. For the three-component TAG nanocomposite, there is a noticeable decrease in the intensity of rutile peaks against a broad amorphous signal in the 1350–1600 cm^{-1} range, where weak D and G bands characteristic of rGO carbon structures are observed. This confirms the successful deposition of reduced graphene oxide on the TiO_2 surface and the formation of a hybrid conductive network. Therefore, Raman spectroscopy data indicate that all samples retain the rutile phase of TiO_2 after modification with Ag and rGO. The change in intensity and broadening of the peaks indicate the formation of interfacial interaction between TiO_2, Ag, and rGO, which may contribute to effective charge separation and increased photocatalytic activity of the TAG nanocomposite.

Fig. 4a provides the normalised absorption spectra of TNR films before and after the deposition of Ag NPs and rGO structures. Measurements were performed in the wavelength range of 300–700 nm. The TNR sample shows an intense absorption peak in the ultraviolet region with a maximum at 340 nm and a fundamental absorption edge at 390–400 nm, which corresponds to the rutile phase of TiO_2. The characteristic shape of the TNR spectrum indicates interzone excitation of electrons from the valence band to the conduction band at energies exceeding the band gap ($Eg \approx 3.3$ eV). The insert below presents the absorption spectra of Ag NPs and rGO nanostructures. The figure shows that Ag NPs have a broad absorption spectrum from 300 to 480 nm with a maximum absorption at 410 nm. rGO nanostructures absorb electromagnetic radiation in the UV region in the range of 200–300 nm with a maximum absorption peak at 226 nm, which is characteristic for graphene oxide.

After modification of the TNR Ag NPs, a noticeable change in the nature of the spectra is observed: an extended absorption 'tail' appears in the 410-430 nm range. The figures demonstrate that with an increase in the concentration of Ag NPs in the nanocomposite, the peak in the 410–430 nm range initially begins to increase (at 2.0 mmol) and then decreases again with an excess of Ag NPs (at 2.5 mmol). It can be related to the SPR phenomenon of Ag NPs, which can effectively absorb photons in the visible range and amplify local electromagnetic fields at the TiO_2/Ag boundary. The resulting collective oscillations of electrons on the surface of Ag particles lead to a broadening of the spectral response of

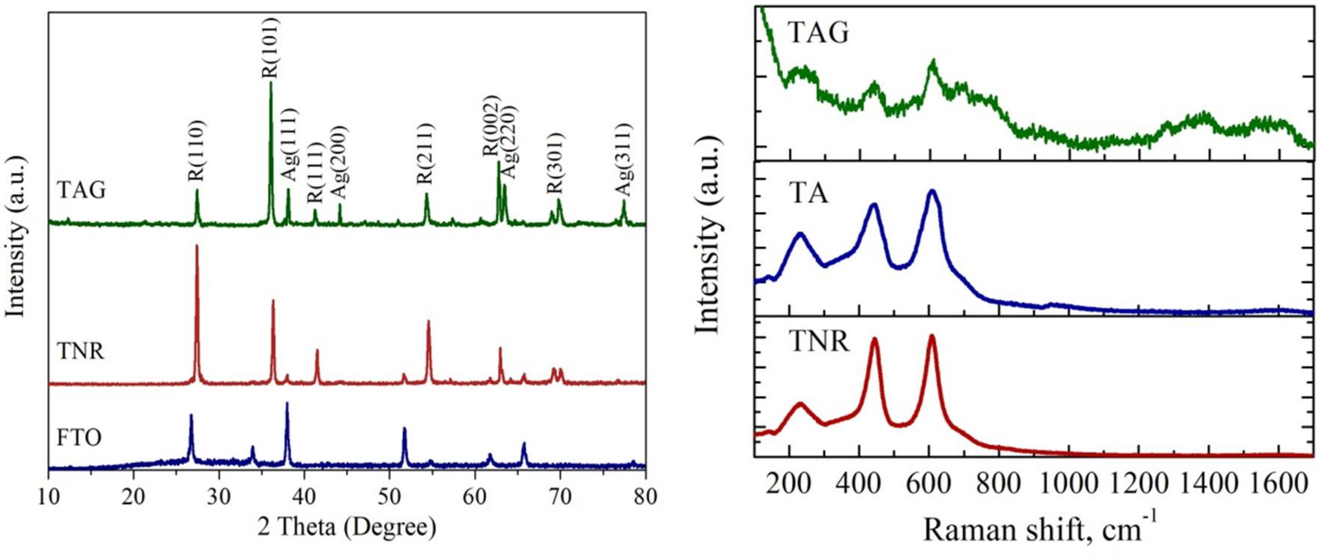

(a) (b)

Fig. 3: XRD spectra (a) and Raman spectra's (b) of TNR, TA и TAG.

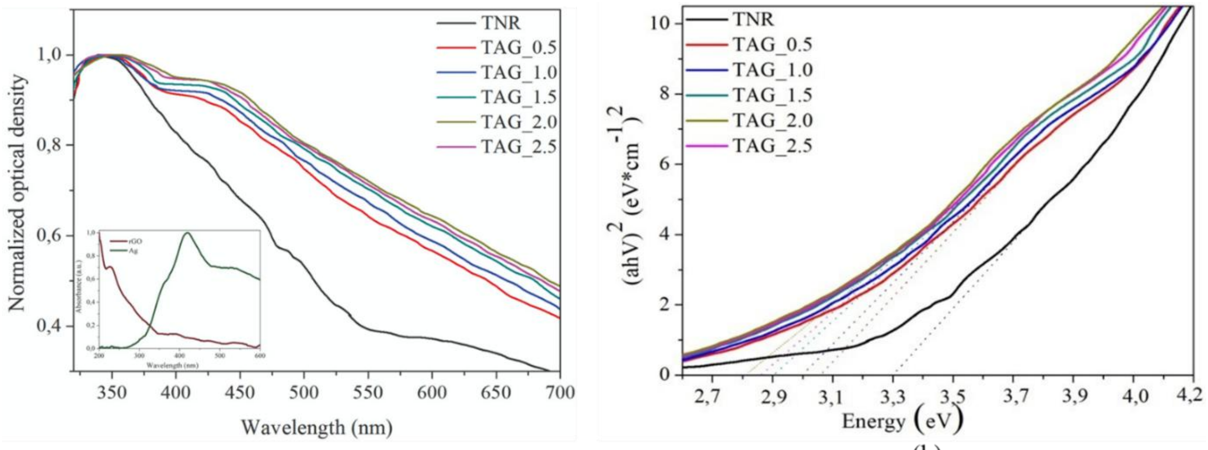

(a) (b)

Fig. 4: Influence of Ag NPs concentration and rGO structures on TNR absorption spectra (a) and their Tauc plot for determining the bandgap width.

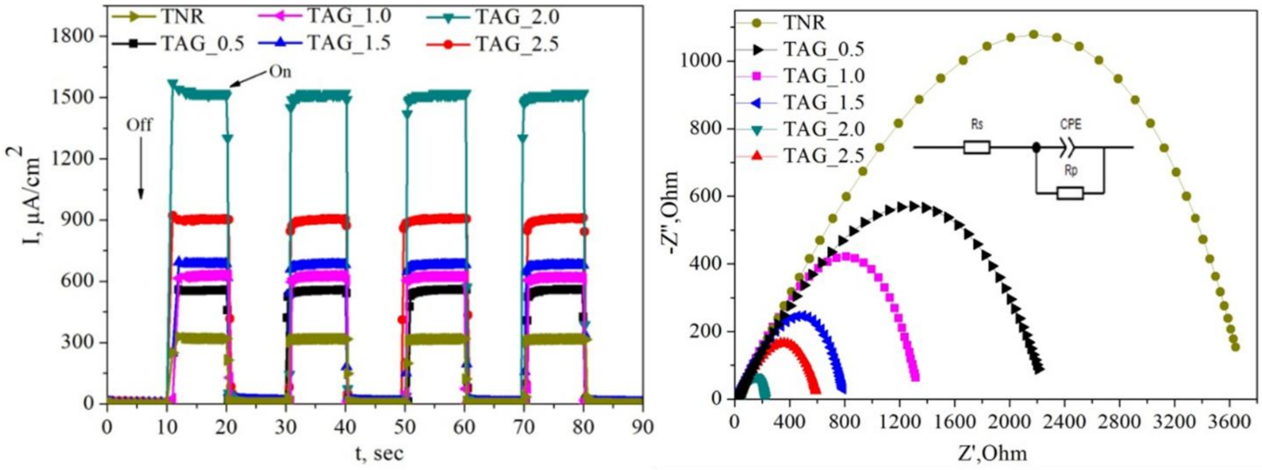

(a) (b)

Fig. 5: Comparative graphs of photocurrent (a) and impedance characteristics (b) of nanocomposites.

the material and a shift of the absorption edge towards longer wavelengths, which results in a reduction in the width of the forbidden zone, as shown in Fig. 4b. The broadband absorption of rGO in the UV range further contributes to the enhancement of overall light absorption. TAG nanocomposites demonstrate absorption across a wide range of wavelengths from UV to visible light. This is associated with the synergistic effect of the interaction of all three components: TiO_2 provides photogeneration of electrons in the UV region, while low-frequency Ag expands the absorption capacity of materials in the visible range due to its own absorption or due to the SPR phenomenon. The Tauc plot (Fig. 4b), constructed using the Kubelka–Munk transformation, shows that an increase in the concentration of Ag NPs in the nanocomposite leads to a decrease in its band gap width. The width of the forbidden zone TNR, TAG_0.5, TAG_1.0, TAG_1.5, TAG_2.0 and TAG_2.5 is 3.3, 3.1, 3.0, 2.9 eV, 2.85 and 2.8 eV, respectively.

Fig. 5a presents the transient characteristics of photocurrent as a function of time for TNR and TAG with different Ag NPs content. The measurements were performed with cyclic switching on/off of the lighting, which allows assessing the stability and repeatability of the photo response of the samples. The samples demonstrate good stability over the time interval under investigation. The photocurrent density is practically zero when the light is off and increases instantly when it is turned on. The data presented shows that when exposed to light, the TNR film generates approximately 326 μA/cm^2. With an increase in the amount of reconstituted Ag NPs and rGO deposition on the TNR surface, the generated photocurrent initially increased, then decreased again after reaching a certain concentration, indicating the presence of an optimal concentration. At TAG_0.5, the generated photocurrent was 500 μA/cm^2, which is 1.5 times higher than that of a pure TNR film. Growth was observed up to sample TAG_2.0, where the photoinduced current value was 1575 μA/cm^2, which is 4.8 times higher than that of TNR. Then, for TAG_2.5, the photocurrent value decreased again and amounted to 920 μA/cm^2. The injection of Ag NPs enhances the photocurrent due to surface plasmon resonance and intrinsic absorption in the visible range of solar radiation, while the deposited rGO sheets facilitate rapid electron transport due to improved conductivity and high charge carrier mobility.

Impedance spectroscopy was used to study the electrical transport properties of TNR nanocomposites with different Ag content and deposited rGO sheets. To this end, according to the methodology specified in paragraph 2, electrochemical cells were assembled and their impedance spectra were measured when the surface was illuminated by a solar radiation simulator (Fig. 5b). Then, using the potentiostat software package with the EIS add-on, a simple equivalent circuit was constructed with a series resistance R_s and a parallel RC circuit connection. After that, the modelled impedance spectra were selected so that they precisely overlapped the surface of the measured impedance spectra. To calculate the resistance parameters and effective electron lifetime, the technique described in Adachi *et al*. was used.[42]

According to the model, the peak frequency of the arc w_{max} in the Nyquist plot is related to the effective electron recombination rate constant k_{eff} via the ratio $w_{max} = k_{eff}$ and the diameter of the arc allows the interphase charge transfer resistance R_p to be estimated. The R_s value corresponds to the total ohmic resistance of the system, including the electrolyte and contacts. The effective lifetime of electrons is defined as: $\tau_{eff} = 1/k_{eff}$. The results of the calculations are recorded in Table 1.

Table 1: Electrical characteristics of samples calculated from the impedances of the Nyquist diagram.

Sample	R_s, Ohm	R_p, Ohm	k_{eff}, s^{-1}	τ_{eff}, s
TNR	47.2	3690.0	0.85	1.17
TAG_0.5	22.5	2256.0	1.35	0.74
TAG_1.0	31.5	1316.6	1.53	0.65
TAG_1.5	24.5	777.8	1.67	0.59
TAG_2.0	43.4	177.9	2.40	0.42
TAG_2.5	20.9	584.6	2.10	0.47

TNR films are characterised by high transfer resistance of charge carriers and have an R_p value of 3690 Ohms, which indicates limited electron transport and a high degree of recombination. The tabulated data demonstrate that with an increase in the concentration of Ag NPs in the TNR and rGO system, there is a significant decrease in the resistance to charge carrier transport and a reduction in the effective lifetime of electrons in the excited state. The resistance to charge carrier transport was reduced by a factor of 20 times compared to the initial TNR film. This may be due to a several reasons: firstly, metallic Ag NPs and rGO sheets have high conductivity, and their incorporation into the TNR film leads to a decrease in resistance; secondly, photoexcited electrons of Ag NPs in the visible region of electromagnetic radiation and the SPR effect effectively populate the conduction band of TNR with free electrons, and the embedded rGO sheets contribute to the effective removal of these electrons, which can lead to a decrease in the overall resistance of the nanocomposite material. Furthermore, the tabulated data shows that the effective lifetime of electrons in the excited state decreases, which may also be related to the electron removal rate.

The photocatalytic activity of nanocomposite materials was evaluated based on the photodegradation of MB, CR and RhB dyes. The degree of dye degradation was monitored by changes in optical density at the maximum absorption band: for MB – 662 nm, for CR – 498 nm, and for RhB – 522 nm (Fig. 6).

Before measuring photodegradation, all samples were pre-incubated in solutions for 12 hours in the dark to eliminate errors associated with the physical adsorption of dye onto the surface of the photocatalyst. The initial concentration of the dye is 10–5 mol/l. The volume of the solution was 10 ml. The measurements were carried out in a quartz cuvette. When dye was irradiated without the presence of photocatalysts, degradation was lower than when a photocatalyst was present, and after 240 minutes of irradiation, the degree of degradation was 20% for MB, 1.8% for CR, and 70% for RhB. Next, when immersed in the photocatalyst solution, the degree of dye degradation increased. At the same time, with an increase in the concentration of Ag NPs (up to sample TAG_2.0) in the TNR and rGO system, an increase in the degradation rate of all three dyes is observed. Then, upon reaching the optimal concentration (for sample TAG_2.5), the degradation rate slows down again. Thus, for sample TAG_2.0, the degree of dye degradation after 240 minutes of irradiation is: for MB – 64%, for CR – 5.6% and for RhB – 94%. The remaining samples occupied intermediate values. This circumstance allows to conclude that the introduction of the optimal concentration of Ag NPs into the TNR and rGO system accelerates the photodegradation of MB, CR and RhB dyes by 3.2, 3.1, and 1.4 times, respectively, compared to when the photocatalyst was absent in the dye.

The mechanism of photodegradation of dyes is associated with the generation of active oxygen species. In particular, electron-hole transitions are generated when incident photons are absorbed by a semiconductor. In this case, the holes in the valence band of TiO_2 react with surface H_2O molecules and form hydroxyl radicals ($OH^\bullet$), as shown in Fig. 7.

Under the influence of solar photons with energy exceeding Eg, electrons are excited from the valence band (VB) to the conduction band (CB) of the TNR. rGO serves as a conductive grid: accepts photoelectrons from TiO_2 Ag NPs and transports them, reducing the probability of recombination. Ag NPs create an SPR effect, amplifying the local electromagnetic field and potentially accelerating electron transfer.[43] Key redox reactions occur on the surface of the catalyst, forming superoxide anion radicals ($O_2^{\bullet -}$) and hydroxyl radicals ($^\bullet OH$) — the main oxidants. The radicals $^\bullet OH$ and $O_2^{\bullet -}$ interact with dye molecules, breaking their bonds. The more light the photocatalyst absorbs, the more free electrons will be generated, which participate in redox

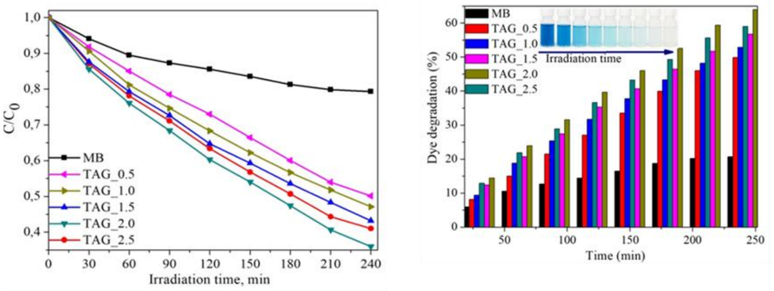

a) MB

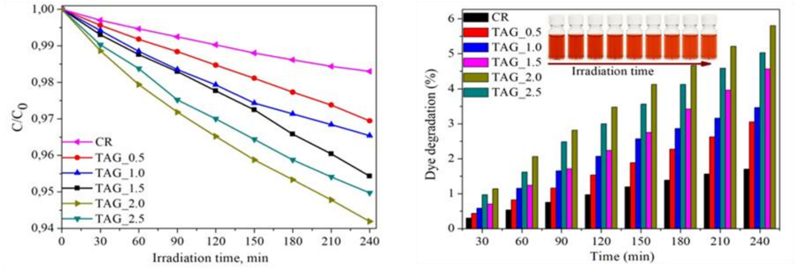

b) CR

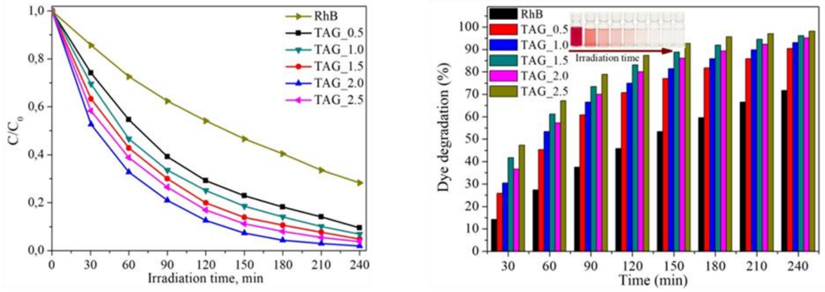

c) Rhb

Fig. 6: Photodegradation kinetics and degree of decomposition of MB, CR and RhB dyes in the presence of TNR nanocomposites and rGO sheets with different concentrations of Ag NPs

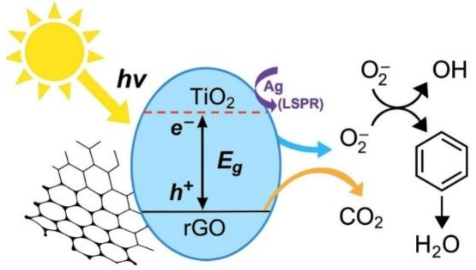

Fig. 7: Schematic representation of the photocatalysis mechanism of TAG nanocomposite.

reactions. Thus, based on the results of the experiments conducted, it has been established that the introduction of Ag NPs and a conductive layer of rGO into the TNR system leads to an increase in the photocatalytic activity of the film. At the same time, there is an optimal concentration of Ag NPs (TAG_2.0) in the composition of TNR and rGO, at which the best generation of photocurrent and photodegradation of MB, CR and RhB dyes is observed, making TAG_2.0 a promising material for the treatment of wastewater from persistent organic dyes under the influence of solar radiation.

4. Conclusion

The influence of Ag NPs concentration on the photocatalytic activity of TNR and rGO nanocomposites was investigated. TNRs were obtained by hydrothermal synthesis. The concentration of Ag NPs on the surface of TNR films was controlled by chemically reducing $AgNO_3$ with different molar masses: 0.5, 1.0, 1.5, 2.0 and 2.5 mmol. rGO nanostructures are deposited onto the surface of TNR/Ag by electrochemical deposition from a phosphate buffer solution. SEM surface morphology analysis confirmed the formation of TNRs with a length of ~3.2 μm and a diameter of 50-70 nm. The EDA showed that as a result of chemical reduction of $AgNO_3$ with different molar masses, spherical Ag NPs with different concentrations and diameters of 5–12 nm are formed on the surface of TNR. In addition, the figures clearly demonstrate the precipitated rGO structures. XRD data indicated that TNR is a rutile modification. With the addition of Ag NPs to TNR, peaks characteristic of Ag are additionally recorded. Raman spectroscopy identified three Raman modes corresponding to the B_{1g}, E_g, and A_{1g} vibrational modes of the rutile phase of TiO_2, and the Raman scattering peaks at 1350–1600 cm^{-1}, where weak D and G bands are observed, are characteristic of rGO carbon structures. Measurement of absorption spectra and Tauc plots constructed using the Kubelka–Munk transformation showed that the maximum of the TNR absorption peak is in the UV region at around 340 nm, and the edge of the fundamental absorption is at 390–400 nm. When introduced into the structure of Ag NPs and rGO nanostructures, their absorption in the range of 410-430 nm appears. Selection of the optimal concentration of Ag NPs and deposition of rGO made it possible to improve the absorption capacity of TAG and reduce its band gap from 3.3 eV to 2.8 eV. The photocatalytic activity of the samples was assessed by the transient characteristics of the photocurrent depending on time and photodegradation of MB, CR and RhB dyes. Selection of the optimal concentration of deposited Ag NPs and deposition of rGO on the TNR surface made it possible to increase the photoinduced current by 4.8 times compared to TNR. At the same time, this made it possible to accelerate the photodegradation of MB, CR and RhB dyes by 3.2, 3.1 and 1.4 times, respectively, compared to when there was no photocatalyst in the dye. Using impedance spectroscopy, it was found that with an increase in the concentration of Ag NPs in the TNR and rGO system, there is a significant decrease in the resistance to charge carrier transfer (by 20 times) and a decrease in the effective lifetime of electrons (by 2.7 times) compared to the original TNR film. The decrease in resistance may be due to the presence of both the intrinsic conductivity of Ag NPs and the presence of absorption capacity in the visible range and the operation of the SPR effect, which generate free electrons. Introduction of rGO sheets facilitate the efficient removal of these electrons, forming heterojunctions that facilitate effective charge carrier separation. Thus, the obtained results confirm that the introduction of optimized amounts of Ag NPs and rGO provides a pronounced synergistic effect, enhancing the photocatalytic activity of the TAG nanocomposite under solar radiation. This makes the material promising for use in wastewater treatment processes and other photocatalytic technologies.

Acknowledgments

This work was supported by the Science Committee of the Ministry of Science and Higher Education of the Republic of Kazakhstan [Grant No. AP23487860].

Conflict of Interest

There are no conflicts to declare.

Supporting Information

Not applicable.

CRediT Statement

A. Kayumova: Resources, Investigation, Writing – Original draft. **P. Zhanbirbayeva:** Investigation, Formal analysis. **A. Kuanyshbekova:** Methodology, Investigation. **A. Baltabekov:** Visualization, Validation, Writing – Original draft. **N. Ibrayev:** Conceptualization, Methodology, Resources, Writing – Review and editing. **N. Ibrayev:** Conceptualization, Writing – Review and editing. **T. Serikov:** Methodology, Investigation, Writing – Original draft. The final manuscript was read and approved by all authors.

References

[1] L. Lin, H. Yang, X. Xu, Effects of water pollution on human health and disease heterogeneity: a review, *Frontiers in Environmental Science*, 2022, **10**, 880246, doi: 10.3389/fenvs.2022.880246.

[2] S. Dutta, B. Gupta, S. K. Srivastava, A. K. Gupta, Recent advances on the removal of dyes from wastewater using various adsorbents: a critical review, *Materials Advances*, 2021, **2**, 4497-4531, doi: 10.1039/d1ma00354b.

[3] R. Al-Tohamy, S. S. Ali, F. Li, K. M. Okasha, Y. A. G. Mahmoud, T. Elsamahy, H. Jiao, Y. Fu, J. Sun, A critical review on the treatment of dye-containing wastewater: Ecotoxicological and health concerns of textile dyes and possible remediation approaches for environmental safety, *Ecotoxicology and Environmental Safety*, 2022, **231**, 113160, doi: 10.1016/j.ecoenv.2021.113160.

[4] A. Othmani, S. Magdouli, P. Senthil Kumar, A. Kapoor, P. V. Chellam, Ö. Gökkuş, Agricultural waste materials for adsorptive removal of phenols, chromium (VI) and cadmium (II) from wastewater: a review, *Environmental Research*, 2022, **204**, 111916, doi: 10.1016/j.envres.2021.111916.

[5] A. Kumar, P. Choudhary, A. Kumar, P. H. C. Camargo, V. Krishnan, Recent advances in plasmonic photocatalysis based on TiO_2 and noble metal nanoparticles for energy conversion, environmental remediation, and organic synthesis, *Small*, 2022, **18**, 2101638, doi: 10.1002/smll.202101638.

[6] C. Hu, S. Tu, N. Tian, T. Ma, Y. Zhang, H. Huang, Photocatalysis enhanced by external fields, *Angewandte Chemie International Edition*, 2021, **60**, 16309-16328, doi: 10.1002/anie.202009518.

[7] C. Zhao, T. Jing, M. Dong, D. Pan, J. Guo, J. Tian, M. Wu, N.

Naik, M. Huang, Z. Guo, A visible light driven photoelectrochemical chloramphenicol aptasensor based on a gold nanoparticle-functionalized 3D flower-like MoS_2/TiO_2 heterostructure, *Langmuir*, 2022, **38**, 2276-2286, doi: 10.1021/acs.langmuir.1c02956.

[8] C. Damm, G. Israel, Photoelectric properties and photocatalytic activity of silver-coated titanium dioxides, *Dyes and Pigments*, 2007, **75**, 612-618, doi: 10.1016/j.dyepig.2006.07.009.

[9] Y. Yamazaki, M. Fujitsuka, S. Yamazaki, Effect of organic additives during hydrothermal syntheses of rutile TiO_2 nanorods for photocatalytic applications, *ACS Applied Nano Materials*, 2019, **2**, 5890-5899, doi: 10.1021/acsanm.9b01334.

[10] B. Liu, J. E. Boercker, E. S. Aydil, Oriented single crystalline titanium dioxide nanowires, *Nanotechnology*, 2008, **19**, 505604, doi: 10.1088/0957-4484/19/50/505604.

[11] Y. Yamazaki, K. Azami, R. Katoh, S. Yamazaki, Developing active TiO_2 nanorods by examining the influence of morphological changes from nanorods to nanoparticles on photocatalytic activity, *ACS Applied Nano Materials*, 2018, **1**, 5927-5935, doi: 10.1021/acsanm.8b01617.

[12] W. Fang, M. Xing, J. Zhang, Modifications on reduced titanium dioxide photocatalysts: a review, *Journal of Photochemistry and Photobiology C: Photochemistry Reviews*, 2017, **32**, 21-39, doi: 10.1016/j.jphotochemrev.2017.05.003.

[13] T. M. Serikov, The effect of electric transport properties of titanium dioxide nanostructures on their photocatalytic activity, *Bulletin of the Karaganda University "Physics Series"*, 2020, **99**, 13-21, doi: 10.31489/2020ph3/13-21.

[14] P. D. Cozzoli, A. Kornowski, H. Weller, Low-temperature synthesis of soluble and processable organic-capped anatase TiO_2 nanorods, *Journal of the American Chemical Society*, 2003, **125**, 14539-14548, doi: 10.1021/ja036505h.

[15] S. S. Mandal, A. J. Bhattacharyya, Electrochemical sensing and photocatalysis using Ag–TiO_2microwires, *Journal of Chemical Sciences*, 2012, **124**, 969-978, doi: 10.1007/s12039-012-0290-9.

[16] T.-L. Guo, J.-G. Li, X. Sun, Y. Sakka, Photocatalytic growth of Ag nanocrystals on hydrothermally synthesized Multiphasic TiO_2/reduced graphene oxide (rGO) nanocomposites and their SERS performance, *Applied Surface Science*, 2017, **423**, 1-12, doi: 10.1016/j.apsusc.2017.06.151.

[17] C. Y. Ma, J. L. Wang, C. Leng, N. Zhou, F. W. Qin, Q. Y. Zhang, Structural, morphological, optical and photocatalytic properties of Ag decorated graphene oxide-TiO_2 films, *Thin Solid Films*, 2021, **724**, 138632, doi: 10.1016/j.tsf.2021.138632.

[18] A. S. Kayumova, Effect of the concentration of silver nanoparticles on the photocatalytic activity of titanium dioxide nanorods, *Eurasian Physical Technical Journal*, 2023, **20**, 39-45, doi: 10.31489/2023no4/39-45.

[19] J. Z. Soo, L. C. Chai, B. C. Ang, B. H. Ong, Enhancing the antibacterial performance of titanium dioxide nanofibers by coating with silver nanoparticles, *ACS Applied Nano Materials*, 2020, **3**, 5743-5751, doi: 10.1021/acsanm.0c00925.

[20] Q. Zhu, K. Zhang, Y. Huang, R. Liu, Y. Pan, H. Zhang, P. Wang, S. Zhang, D. Pan, Z. Guo, Hydrothermally synthesized ZnO-reduced graphene oxide nanocomposite for enhanced anticorrosion performance of waterborne epoxy coating, *Journal of Nanostructure in Chemistry*, 2022, **12**, 277-289, doi: 10.1007/s40097-022-00470-9.

[21] M. N. Mustafa, N. A. Azhari, Y. Sulaiman, Reduced graphene oxide-titanium dioxide compact layer prepared *via* electrodeposition for enhanced performance of dye-sensitized solar cells, *Optical Materials*, 2021, **120**, 111475, doi: 10.1016/j.optmat.2021.111475.

[22] J. Corredor, M. J. Rivero, I. Ortiz, New insights in the performance and reuse of rGO/TiO_2 composites for the photocatalytic hydrogen production, *International Journal of Hydrogen Energy*, 2021, **46**, 17500-17506, doi: 10.1016/j.ijhydene.2020.01.181.

[23] E. C. Doluel, U. Kartal, T. Dikici, M. Yurddaskal, Effect of Ag content on photocatalytic activity of Ag@TiO_2/rGO hybrid photocatalysts, *Journal of Electronic Materials*, 2020, **49**, 3849-3859, doi: 10.1007/s11664-020-08102-0.

[24] G. Liu, Z. Xiong, L. Yang, H. Shi, D. Fang, M. Wang, P. Shao, X. Luo, Electrochemical approach toward reduced graphene oxide-based electrodes for environmental applications: a review, *Science of The Total Environment*, 2021, **778**, 146301, doi: 10.1016/j.scitotenv.2021.146301.

[25] Zh. Jie, X. Xiao, Y. Huan, H. Youkang, Zh. Zhiyao, The preparation and characterization of TiO_2/rGO/Ag nanocomposites and its photocatalytic activity in formaldehyde degradation, *Environmental Technology*, 2019, **42**, 193-205, doi: 10.1080/09593330.2019.1625955.

[26] H. Deng, H. He, S. Sun, X. Zhu, D. Zhou, F. Han, B. Huang, X. Pan, Photocatalytic degradation of dye by Ag/TiO_2 nanoparticles prepared with different Sol–gel crystallization in the presence of effluent organic matter, *Environmental Science and Pollution Research*, 2019, **26**, 35900-35912, doi: 10.1007/s11356-019-06728-0.

[27] M. Sheydaei, B. Ayoubi-Feiz, Nitrate reduction through the visible-light photoelectrocatalysis and photoelectrocatalysis/reverse osmosis processes: Assessment of graphene/Ag/N-TiO_2 nanocomposite, *Journal of Water Process Engineering*, 2021, **39**, 101856, doi: 10.1016/j.jwpe.2020.101856.

[28] Md.R. Al-Mamun, Md.N. Karim, N.A. Nitun, Sh. Kader, Md.Sh. Islam, Z.H. Khan, Photocatalytic performance

assessment of GO and Ag co-synthesized TiO_2 nanocomposite for the removal of methyl orange dye under solar irradiation, *Environmental Technology & Innovation*, 2021, **22**, 101537, doi: 10.1016/j.eti.2021.101537.

[29] H. Chakhtouna, H. Benzeid, N. Zari, A. el kacem Qaiss, R. Bouhfid, Recent progress on Ag/TiO_2 photocatalysts: photocatalytic and bactericidal behaviors, *Environmental Science and Pollution Research*, 2021, **28**, 44638-44666, doi: 10.1007/s11356-021-14996-y.

[30] B. Gupta, A. A. Melvin, TiO_2/RGO composites: Its achievement and factors involved in hydrogen production, *Renewable and Sustainable Energy Reviews*, 2017, **76**, 1384-1392, doi: 10.1016/j.rser.2017.03.123.

[31] L. Sang, L. Lei, C. Burda, Electrochemical fabrication of rGO-embedded Ag-TiO_2 nanoring/nanotube arrays for plasmonic solar water splitting, *Nano-Micro Letters*, 2019, **11**, 97, doi: 10.1007/s40820-019-0329-2.

[32] A. Zhumabekov, T. Dossanov, A. Kassanova, N. Ispulov, A. Iskakova, D. Temirbayeva, Z. Daniyarova, Enhancement of optoelectronic performance by plasmonic effect in TiO_2-rGO/Ag-TiO_2 based on UV detectors, *Physica Scripta*, 2025, **100**, 025935, doi: 10.1088/1402-4896/adab3e.

[33] L. Yu, L. Wang, X. Sun, D. Ye, Enhanced photocatalytic activity of rGO/TiO_2 for the decomposition of formaldehyde under visible light irradiation, *Journal of Environmental Sciences*, 2018, **73**, 138-146, doi: 10.1016/j.jes.2018.01.022.

[34] W. D. Toledo, A. B. Couto, D. L. Almeida, N. G. Ferreira, Facile synthesis of TiO_2/rGO neatly electrodeposited on carbon fiber applied as ternary electrode for supercapacitor, *Materials Research Express*, 2019, **6**, 065040, doi: 10.1088/2053-1591/ab0928.

[35] L. Zhang, C. Ni, H. Jiu, C. Xie, J. Yan, G. Qi, One-pot synthesis of Ag-TiO 2/reduced graphene oxide nanocomposite for high performance of adsorption and photocatalysis, *Ceramics International*, 2017, **43**, 5450-5456, doi: 10.1016/j.ceramint.2017.01.041.

[36] V. P. Parvathi, R. Parimaladevi, V. Sathe, M. Umadevi, Environmental photochemistry by plasmonic semiconductor decorated GO nanocomposites: SERS detection and visible light driven degradation of aromatic dyes, *Applied Surface Science*, 2019, **473**, 864-872, doi: 10.1016/j.apsusc.2018.12.241.

[37] G. Sanzone, M. Zimbone, G. Cacciato, F. Ruffino, R. Carles, V. Privitera, M. G. Grimaldi, Ag/TiO_2 nanocomposite for visible light-driven photocatalysis, *Superlattices and Microstructures*, 2018, **123**, 394-402, doi: 10.1016/j.spmi.2018.09.028.

[38] A.S. Kayumova, T.M. Serikov, G.S. Omarova, Effect of duration of electrochemical deposition of graphene oxide on photocatalytic activity of TiO_2 nanorods, *Bulletin of Toraighyrov University*, 2025, **1**, 195-206, doi: 10.48081/elgd3788.

[39] T. M. Serikov, N. K. Ibrayev, T. M. Ivanova, S. V. Savilov, Influence of the hydrothermal synthesis conditions on the photocatalytic activity of titanium dioxide nanorods, *Russian Journal of Applied Chemistry*, 2021, **94**, 442-449, doi: 10.1134/s1070427221040030.

[40] P. Kumar, A. Sarkar, P. Jain, Green synthesis of reduced graphene oxide nanosheet by using L-ascorbic acid and study of its cytotoxicity on human cervical cancer cell line, *Journal of Polymer Materials*, 2022, **39**, 121-135, doi: 10.32381/jpm.2022.39.1-2.8.

[41] D. Birhan, D. Tekin, H. Kiziltas, Thermal, photocatalytic, and antibacterial properties of rGO/TiO_2/PVA and rGO/TiO_2/PEG composites, *Polymer Bulletin*, 2022, **79**, 2585-2602, doi: 10.1007/s00289-021-03914-4.

[42] M. Adachi, M. Sakamoto, J. Jiu, Y. Ogata, S. Isoda, Determination of parameters of electron transport in dye-sensitized solar cells using electrochemical impedance spectroscopy, *The Journal of Physical Chemistry B*, 2006, **110**, 13872-13880, doi: 10.1021/jp061693u.

[43] M. Khairy, E. M. Kamar, M. A. Mousa, Photocatalytic activity of nano-sized Ag and Au metal-doped TiO_2 embedded in rGO under visible light irradiation, *Materials Science and Engineering: B*, 2022, **286**, 116023, doi: 10.1016/j.mseb.2022.116023.

Open Access